11th International Conference on Vibration Problems
Z. Dimitrovová *et.al.* (eds.)
Lisbon, Portugal, 9–12 September 2013

MEASUREMENT AND SIMULATION OF MACHINE-BORNE VERTICAL VIBRATION IN ELEVATOR SYSTEMS

X. Arrasate*[1], S. Kaczmarczyk[2], G. Almandoz[3], J.M. Abete[4], I. Isasa[5]

[1]Applied Mechanics, Mondragon Unibertsitatea, 20500 Arrasate/Mondragon, Euskadi, Spain
jarrasate@mondragon.edu

[2]Department of Engineering and Technology, School of Science and Technology, University of Northampton, St. Georges Avenue, Northampton NN2 6JD, UK
Stefan.Kaczmarczyk@northampton.ac.uk

[3]Electric Drives, Mondragon Unibertsitatea, 20500 Arrasate/Mondragon, Euskadi, Spain
galmandoz@mondragon.edu

[4]Applied Mechanics, Mondragon Unibertsitatea, 20500 Arrasate/Mondragon, Euskadi, Spain
jmabete@mondragon.edu

[5]Mechanical Engineering, Orona EIC S. Coop. Elevator Innovation Center, 20120 Hernani, Euskadi, Spain
iisasa@orona-group.com

Keywords: Elevator, Vertical Vibration, Electric Machine, Simulation, Measurement.

Abstract. *In this paper vertical vibration measurements performed on a laboratory model of an elevator system have been presented and analysed. The laboratory model consists of a machine system that drives two rigid masses representing an elevator car and a counterweight, constrained by guide rails to move vertically through a sheave and hoist rope. Simultaneous measurements to record accelerations of the masses and of the machine are conducted. The three phase current intensities and the velocity signal provided by the encoder are also recorded during the travels. The machine torque is computed from the current intensities and the motor torque ripple is analysed. A mathematical model of the laboratory setup that includes the drive system (machine and controllers) is developed to simulate the system response. A five-degree-of-freedom lumped-parameter model of the car-counterweight-sheave-rope assembly is developed. The modulus of elasticity of the rope and the friction coefficients at the guide rail contact and at the machine shaft are estimated from the experimental tests. When simulating a travel, the measured torque ripple is added to the controller generated torque as a perturbation. The acceleration response obtained from the simulations and that one obtained in the measurements are similar in amplitude and frequency content. Both show that the car frame vibrates particularly at those excitation frequencies close to the natural frequencies of the elevator system model.*

1 INTRODUCTION

One of the main problems in elevator installations is to achieve and maintain adequate ride quality standards. Car ride quality can be compromised by excessive vibrations. Hoist ropes due to their flexibility and loading conditions are particularly affected. The drive machine is the source of energy supplied to the system but it is as well a source of excitations such as imbalance of the machine, eccentricity of the traction sheave or the electromagnetic torque ripple.
The elevator system can be considered as a translating assembly of inertia elements coupled and constrained by one-dimensional slender continua. The inertia elements are the rotating components of the machine, the car assembly, the counterweight and the traction sheave. The one-dimensional slender continua are the suspension ropes that may vibrate laterally and vertically.
It is often assumed that the coupling between the vertical and the lateral vibration can be neglected (because the lateral vibration amplitude is assumed to be small, which is the case when the rope tension is high) and, consequently, vertical vibration is studied independently [1].
The suspension rope can be represented by a lumped-mass model with point masses joined by springs and dampers with the corresponding stiffness and damping coefficients [2]. Such models are described by a set of ODEs. The number of discrete mass points corresponds to the number of degrees of freedom (DOF) of the system and to the number of natural frequencies and mode shapes that are considered. This approach enables to simulate the vertical vibration during a travel by updating the models at every time step [3].
In this work, vertical vibrations of an elevator car caused by excitations generated at a synchronous motor are investigated.
Experimental tests are performed using a laboratory model of an elevator system with a 1:1 roping configuration. Then, the acceleration responses of the main components of the model, the three phase current intensities that feed the machine and the rotational velocity of the shaft are measured during a number of travels.
Furthermore, a mathematical model of an elevator is developed in order to predict and to analyse the system response. It includes a comprehensive representation of the drive system and the mechanical part is represented as a 5-DOF lumped-parameter model.
Finite Element Method (FEM) simulation tests by means of the software FLUX are conducted to estimate the machine parameter values, the torque ripple and the radial forces at the machine air-gap. The FLUX computed torque ripple excitation is compared to the torque ripple signal estimated from the values of the intensities of the phase currents. The latter is added as a perturbation to the controller generated torque.
Damping coefficients of the system are estimated from measured acceleration signals.
The ODE set obtained is solved numerically to simulate the response of the elevator components. The experimental and simulation results obtained are then compared and discussed.

2 Elevator System Model

The elevator model that has been developed to simulate the vertical dynamic response of the elevator system to excitations generated at the drive system is composed of two main parts: the drive system and the the car-sheave-counterweight-rope assembly.

2.1 Drive System Model

The input to the drive system is a desired velocity profile and the output is the machine torque, which subsequently forms an input to the mechanical system. The drive system com-

prises a permanent magnet synchronous motor (PMSM) powered via an inverter that supplies a pulse width modulated (PWM) voltage.
The motor shaft speed is controlled in order for the car to follow a prescribed velocity profile ω_{m}^{*} to achieve good ride quality. A well known vector control strategy oriented to the magnets flux has been implemented in the computer simulation [4].

2.2 Vertical vibration model

The assembly composed of the car, the counterweight, the sheave and the ropes is represented by a 5 DOF lumped-parameter model as shown in Fig. 1.

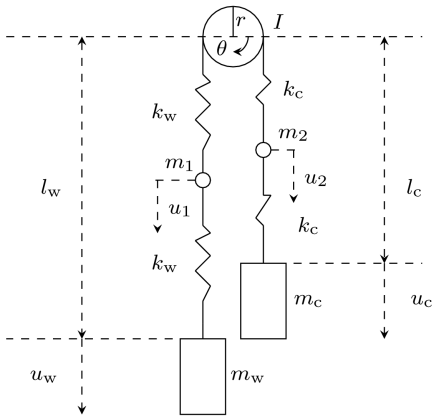

Figure 1: 5 DOF model of a 1:1 roping cfg. elevator

The car, counterweight and sheave inertia are lumped at their corresponding positions; the counterweight-side and car-side rope masses are lumped at discrete points and then jointed to the sheave and counterweight, the sheave and the car, by mass-less springs of stiffness coefficients given by Eqn. 1 and Eqn. 2 respectively

$$k_{\mathrm{w}} = \frac{2EA}{l_{\mathrm{w}}} \tag{1}$$

$$k_{\mathrm{c}} = \frac{2EA}{l_{\mathrm{c}}} \tag{2}$$

where l_{w} and l_{c} are the lengths of the counterweight- and car-side ropes respectively. The configuration of the system is described by five generalized coordinates representing the counterweight, car and counterweight-side and car-side rope mass displacements with respect to the equilibrium position and the displacement of any point of the sheave edge: u_{w}, u_{c}, u_1, u_2 and $u_{\mathrm{sh}} = \theta r$ respectively (see Fig. 1).
The spring stiffness constants are updated every time instant during the elevator travel. The sheave rotation angle is related to the lengths of the counterweight-side and car-side ropes by Eqn 3

$$r\frac{\mathrm{d}\theta}{\mathrm{d}t} = -\frac{\mathrm{d}l_{\mathrm{w}}}{\mathrm{d}t} = \frac{\mathrm{d}l_{\mathrm{c}}}{\mathrm{d}t} \tag{3}$$

The torque provided by the machine is composed of two components; the first one accommodates the torque needed to lift the out-of-balance weight given by Eqn. 4

$$\tau^{\mathrm{e}} = (m_{\mathrm{w}} - m_{\mathrm{c}} + m(l_{\mathrm{w}} - l_{\mathrm{c}}))gr \tag{4}$$

and the second one denoted as τ^{d} which represents the dynamic torque and is accommodated in the vector $\mathbf{\Delta F}$ given as

$$\mathbf{\Delta F} = \begin{bmatrix} 0 \; 0 \; \dfrac{\tau^{\mathrm{d}}}{r} \; 0 \; 0 \end{bmatrix}^{\mathrm{T}} \tag{5}$$

The equation of motion is then written as

$$\mathbf{M}\ddot{\mathbf{x}} + \mathbf{C}\dot{\mathbf{x}} + \mathbf{K}\mathbf{x} = \mathbf{\Delta F} \tag{6}$$

where $\mathbf{M}$, $\mathbf{K}$ and $\mathbf{C}$ are the inertia, stiffness and damping matrices respectively. The damping matrix accounts for the friction at the guide-rail contact interfaces and at the sheave.

3 Computer simulation and experimental tests

Experimental tests have been performed on a laboratory model of an elevator system. The schematic of the laboratory model and the experimental setup are shown in Fig. 2.

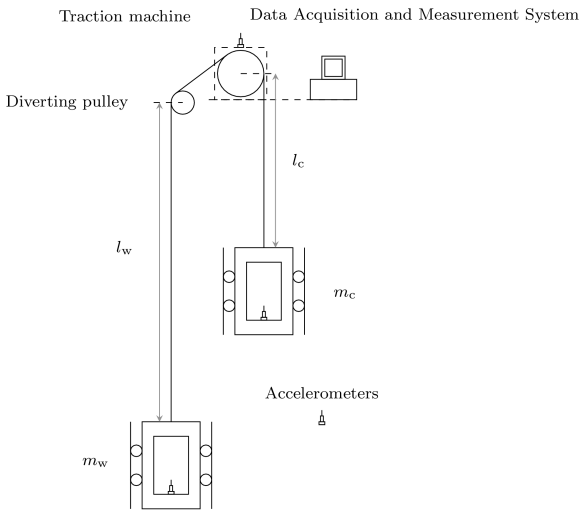

Figure 2: Experimental setup

Two equal rigid rigs are suspended at each side of the traction sheave by one wire rope and guided vertically. A finite element model of the car or counterweight frame assemblies has been developed in order to calculate its natural frequencies with the first natural frequency determined as around 235 Hz.

The suspended rig at the diverting pulley side will be referred to as the car, and that one suspended directly from the traction sheave as the counterweight. Both rigs have got the same mass, 33 kg, but there is the possibility to increase it by placing some weights on them. The length from the counterweight to the traction sheave is l_{w} and that one from the car to the diverting pulley is $l_{\mathrm{c}} = l_{\mathrm{t}} - l_{\mathrm{w}}$, where l_{t} =8.6 m. Other approximate values of the system parameters are I = 0.3385 kg·m^2, r = 0.065 m and $\mu = 0.095$ kg/m.

3.1 Measurement procedure

Three accelerometers, each with its corresponding charge amplifier (see Table 1) have been placed on the frames at the car and at the counterweight side respectively, and on the machine (see Fig. 2).

Acquisition system	B&K Pulse
Accelerometers	B & K 4371, s.n. 1573419
Charge amplifiers	B & K 2635, s.n. 1602883

Table 1: Measurement system

The accelerations have been recorded during a travel together with the encoder signal, proportional to the actual velocity of the machine shaft, and the current intensities of the three phases feeding the machine, measured by current transducers. The sampling frequency has been set as 16384 Hz.
Several tests have been carried out, with the rigs travelling in both directions; the mass of the counterweight has been set as $m_{\mathrm{w}} = 33$ kg in all the tests and the mass of the car m_{c} has taken four different values: 33, 45.5, 58 and 70.5 kgs.

3.2 Computation of the motor parameters and torque ripple amplitude by Finite Element Analysis

The electric motor model uses some characteristic parameters such as inductances, resistance, magnet flux linkage and torque constants. All those parameters of the motor have been computed by Finite Element Analysis (FEA) by means of the software FLUX.
The torque ripple is composed of two components mainly: the electromagnetic torque ripple, due to the spatial distribution of stator windings and the magnets shape, and the cogging torque, due to the number of stator slots and pole pairs [5]. The main electromagnetic torque ripple and the cogging torque frequency values are respectively k =6 and $n = 12$ times the stator current frequency w_{s}, called the fundamental frequency. The fundamental frequency ω_{s} satisfies the following equation,

$$\omega_{\mathrm{s}} = p\omega_{\mathrm{m}} \tag{7}$$

where p is the number of pole pairs of the machine stator and ω_{m} is the rotational speed of the rotor.
Radial magnetic forces at the machine air-gap could be an additional cause of torque ripple. The radial magnetic force per unit area or magnetic pressure waveform at any point of the air gap is obtained by means of the Maxwell's stress tensor theorem [6] given as

$$P_{\mathrm{rd}}(\theta, t) = \frac{1}{2\mu_0}\left(B_{\mathrm{n}}^2(\theta, t) - B_{\mathrm{tg}}^2(\theta, t)\right) \tag{8}$$

where θ is the rotation angle with respect to the axis of symmetry of the machine, μ_0 is the magnetic permeability, t is the time, and B_{n} and B_{tg} the normal and the tangential components of magnetic field around the air-gap. The waveform of the magnetic radial pressure at a certain point of the stator core as a function of the rotor position has been calculated. As it is a p =6 pole pair motor, the spatial period of this signal is $\pi/3$. In its corresponding Fourier series, the highest component corresponds to the spatial order 0 and it is a constant pressure; the spatial

order 2 is a sinusoidal pressure distribution of spatial period $\pi/6$ and corresponding excitation frequency twice the fundamental one, $2w_{\mathrm{s}}$, and it is the main harmonic of the radial force.

3.3 Measured torque ripple

Fig. 3 shows the reference velocity (of a sheave edge point) and counterweight-side rope length time profiles corresponding to one of the test travels; in this particular case, m_{w} =33 kg and m_{c} =70.5 kg. The velocity profile is composed of acceleration and deceleration stages and a constant velocity stage when the system travels at the speed of around 0.4 m/s.

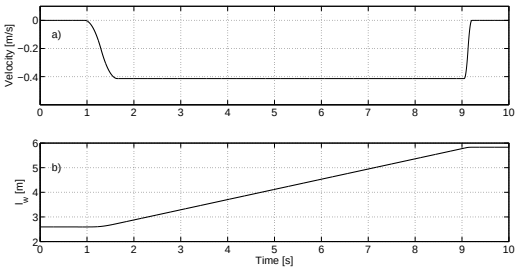

Figure 3: Reference a) velocity and b) counterweight-side rope length

The machine torque has been estimated from the measured three phase current intensities by means of the quadrature zero (dqo) transformation theory [7].
Fig. 4 shows the average power spectral density of the torque ripple during the constant velocity stage. The main electromagnetic torque ripple and the cogging torque frequency values are respectively k =6 and n = 12 times the fundamental frequency w_{s}. Those components and the main component of the radial force, 36, 72 and 12 Hz respectively, are apparent, but there are also components at 1 Hz, due to a possible machine imbalance, 6 Hz, the fundamental frequency, and some of its harmonics (18 Hz, 24 Hz). The actual amplitudes of the electromagnetic (36 Hz) and cogging torque (72 Hz) components obtained from the measured current intensities are around 0.3 Nm and 0.5 Nm respectively and differ from the amplitudes calculated by FEA (see Table **??**). The amplitudes of the frequency components at 1 Hz, 6 Hz and 12 Hz are around 2 Nm, 0.3 Nm and 3.5 Nm respectively.

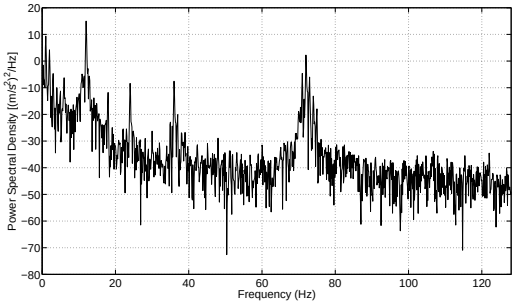

Figure 4: Torque ripple average power spectral density in the constant velocity stage

3.4 Modulus of elasticity of the rope

Experimental tests have been carried out in order to determine the value of the product of the modulus of elasticity of the rope and the cross-section area EA. The determination of the value of E is based on the characteristic equation (Eqn. 9) that gives the natural frequencies of a system that consists of a rope with a fixed end and a suspended mass at the other end ([1]).

$$m_{\mathrm{c}}\gamma_n \sin(\gamma_n l) - m\cos(\gamma_n l) = 0 \tag{9}$$
$$f_n = \frac{1}{2\pi}\gamma_n\sqrt{\frac{EA}{m}}$$

where l is the length of the rope and f_n the nth natural frequency. According to the system described by Eqn. 9, the machine is not working and the rope top end is fixed. The sensors used are given in Table 1. The transient acceleration responses of the suspended mass, for different mass values and rope lengths are measured and the system first natural frequency and corresponding damping ratio are identified from the acceleration signal power spectrum. The values of the product EA for the different suspended masses have been obtained and it has been concluded that as the tension of the rope increases the value of EA increases as well. The slope of the curve decreases as the value of the mass increases.
An average value of $EA = 10^6$ N has been assumed in the simulations.

3.5 Natural frequencies and mode shapes

The natural frequencies and mode shapes of the system have been calculated. The eigenvalue problem that determines the natural frequencies and mode shapes of the system is stated as

$$-\mathbf{K}\mathbf{u} = \mathbf{M}\omega^2\mathbf{u} \tag{10}$$

where $\mathbf{u}$ is the modal vector.
Fig. 5 shows the five natural frequencies calculated by the model.

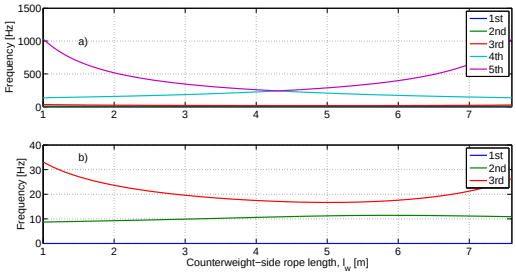

Figure 5: The five natural frequencies as a function of the counterweight-side rope length calculated by the LPM

3.6 Experimental results

Fig. 7 shows the car acceleration (as well as the simulated one) recorded during the travel described in section 3.3, where the counterweight and car masses were m_{w} =33 kg and m_{c} =70.5 kg respectively and the velocity profile was given by Fig. 3 (a). Frequencies below 1 Hz have been filtered out.

Fig. 6 shows the spectrogram of the acceleration measured by the sensor placed on the car. The spectrogram, in dB/Hz (dB relative to the reference value of 1 m/s^2), has been calculated by the Burg algorithm [8]. The frequency band shown corresponds to the interval 0-128 Hz. The natural frequencies of the system in that band have been traced as well.
The main electromagnetic torque ripple and the cogging torque frequency, 36 Hz and 72 Hz respectively, are manifest. Furthermore, the 2nd order component of the radial force is around 12 Hz. All these frequencies appear in the spectrogram shown in Fig. 6. Vibration amplitude at the excitation frequency of 12 Hz is particularly high due to its proximity to the second natural frequency of the system. Fig. 6 shows that during the constant velocity stage the amplitude corresponding to the frequency of around 12 Hz increases progressively; it could be because the 3rd natural frequency gets progressively closer to this frequency.

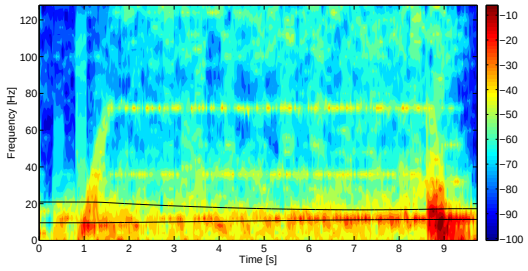

Figure 6: Spectrogram of the acceleration measured on the car

3.7 Simulations

The MATLAB-Simulink software tool has been used to simulate the behaviour of the system during the elevator travel. The reference velocity profile to be followed by the counterweight is given by Fig. 3. The measured torque ripple has been added as a perturbation to the machine torque generated in order to follow the reference velocity profile.

Damping at the rail-guide contact Based on the exponential decrease in the amplitude when the rigs stopped at the end of the travel, the value of the damping factor ζ has been calculated as

$$\zeta = \frac{1}{2\pi} \ln \frac{x(t)}{x(t+T)} \tag{11}$$

where $x(t)$ is the acceleration measured and T its period. The value obtained is around 0.036. The same value of ζ has been assumed for all modes. The values of c_{w} and c_{c} are assumed to be equal and calculated as

$$c_{\mathrm{w}} = c_{\mathrm{c}} = 2\zeta\omega m_{\mathrm{w}} \tag{12}$$

where ω is the circular frequency corresponding to the period T. The value obtained is around 148 kg/s.

Friction and energy losses at the machine Viscous friction and any other possible energy loss at the machine have been accommodated in the parameter c_{sh}. A rough estimate of its value has been obtained by applying the following equation that is satisfied during the constant velocity stage when $m_{\mathrm{c}} = m_{\mathrm{w}}$ and vibrations of the other inertial elements are neglected

$$\tau/r - c_{\mathrm{sh}}\dot{\theta}r - c_{\mathrm{w}}\dot{\theta}r - c_{\mathrm{c}}\dot{\theta}r = 0 \tag{13}$$

where τ is the torque measured at the corresponding travel and $\dot{\theta}$ the shaft velocity. The value obtained is around 3 Nms.

Travel simulation Fig. 7 shows the simulated car acceleration compared to the recorded one. A highpass filter with the cut-off frequency at 1 Hz has been applied to both signals (simulated and measured).

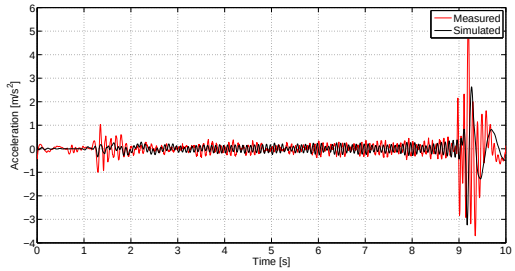

Figure 7: Recorded (red) and simulated (black) car accelerations

The spectrogram of the simulated car acceleration is shown in Fig 8. The excitation frequencies corresponding to the main electromagnetic torque ripple, the cogging and the second order component of the radial force, particularly manifest due to its proximity to the first natural frequency, can be observed. The progressive increase in amplitude during the constant velocity stage at the excitation frequency of 12 Hz that was observed in the acceleration recorded on the car is observed as well in the simulated one (see Fig. 7). Regarding the deceleration stage, in the simulation it is the machine controller that stops the travel, while it is the brake in the experimental tests, causing high vibrations, that are not observed in the simulation results.

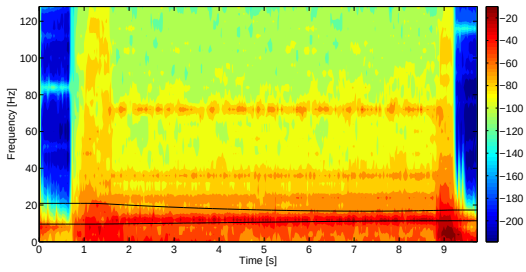

Figure 8: Spectrogram of the car acceleration

4 Conclusions

A laboratory model of an elevator has been developed to validate results obtained from a numerical multi-degree-of-freedom model to predict the response due to excitations generated at the motor drive system. The model includes the drive system, with the machine and its controllers, whose characteristics have been calculated by the electromagnetic FEM software FLUX.

Some parameters of the system are uncertain, i.e. the modulus of elasticity of the rope and the friction coefficients; estimates of their values have been obtained from experimental tests and used in the simulations; the accelerations obtained are similar in the amplitude and frequency content to the corresponding measured dynamic signals. It has been shown that the drive-system borne excitation frequencies close to the elevator system natural frequencies appear in the car- and counterweight-frame acceleration signals.

The proposed simulation model can be used as a design and analysis tool in the development of high-performance elevator systems.

REFERENCES

[1] S. Kaczmarczyk, P. Andrew. Vibration analysis of elevator ropes. *Elevator Technology 14, Proceedings of ELEVCON*, Istanbul, Turkey, 137-144, 2004.

[2] K. Nai, W. Forsythe, R. M. Goodall. Modelling and simulation of a lift system. *Proceedings of the International Conference on Control, Modeling, Computation and Information*, 6–11, 1992.

[3] J. Aldaia, I. Aranburu, J. Pagalday. Mechatronic approach. *Elevator World*, 45(9), 88–92, 1997.

[4] X. Arrasate, S. Kaczmarczyk, G. Almandoz, J.M. Abete, I. Isasa *The Modelling, Simulation And Experimental Testing Of Vertical Vibrations In An Elevator System With 1:1 Roping Configuration*. 2nd Symposium on Lift and Escalator Technologies, Northampton, UK, 2012.

[5] Z. Q. Zhu, S. Ruangsinchaiwanich, Y. Chen, D. Howe. Evaluation of superposition technique for calculating cogging torque in permanent-magnet brushless machines. *IEEE Transactions on Magnetics*, 42(5), 2006.

[6] J. F. Gieras, C. Wang, J. C. Lai. *Noise of polyphase Electric Motors*. Taylor & Francis Group, LLC, 2006.

[7] R. H. Park. Two reaction theory of synchronous machines. *AIEE Transactions*, 48, 716–730, 1929.

[8] J. G. Proakis, D. G. Manolakis. *Digital signal processing*. Prentice Hall, 1996.